Journal of Power Sources 215 (2012) 179–187

Contents lists available at SciVerse ScienceDirect

Journal of Power Sources

journal homepage: www.elsevier.com/locate/jpowsour

The effects of cell assembly compression on the performance of carbon electrochemical double-layer capacitor electrodes

Gerald Gourdin [a], Thomas Jiang [b], Patricia Smith [b], Deyang Qu [a,*]

[a] Department of Chemistry, University of Massachusetts Boston, 100 Morrissey Blvd., Boston, MA 02135, USA
[b] Naval Surface Warfare Center, 9500 MacArthur Blvd., West Bethesda, MD 20817, USA

HIGHLIGHTS

- Increasing force on an EDLC cell only provides a limited increase in the capacitance.
- The force shifts the pore distribution of a porous electrode toward overall smaller pores.
- The surface area which is attributable to small-sized pores is difficult to be accessible.
- Different activated carbons exhibit different behaviors when force was applied to the electrodes.

ARTICLE INFO

Article history:
Received 9 March 2012
Received in revised form
7 April 2012
Accepted 9 April 2012
Available online 4 May 2012

Keywords:
Double-layer supercapacitor
Porosity
Pressure
Accessibility
Kinetics

ABSTRACT

Our previous work concluded that the application of force altered the physical structure of the activated carbon electrodes, which resulted in a decrease in the accessible surface area and a displacement of the electrolyte. In this work, the response that different carbon material electrodes exhibit to an applied force was evaluated. Activated carbon powders possess different porous structures, which would exhibit different behaviors when subjected to an applied force and after the release of that force. Cyclic voltammetry and electrochemical impedance spectroscopy (EIS) were used to characterize the response behaviors of the different carbons. Furthermore, a porosimetry analysis was conducted on the carbon material of the electrode before and after the application of force. It was concluded that the application of force shifted the pore distribution toward overall smaller pores through a compression of the porous structure of the carbon. This resulted in a decrease in the more easily accessible surface area, which was exhibited as a decrease in the capacitance values as calculated from the cyclic voltammetry data. There was no longer sufficient time to access the now smaller powers at the given time scale of the cyclic voltammetry analysis, which negatively impacted the formation of the double layer.

1. Introduction

The energy storage mechanism of electrochemical double-layer capacitors (EDLCs) arises from the electrostatic separation of charge that is established at an electrode/electrolyte interface [1]. Although this mechanism of energy storage provides high power capability it also limits the overall energy density as compared to typical batteries [1,2]. Optimizing the performance for an EDLC can be accomplished through maximizing its volumetric capacitance and reducing its ohmic resistance [3–5]. A common way of accomplishing these goals is to apply a compressing force to the body of the cell during assembly to minimizing the gap between the two electrodes and improve separator/electrode contact. The choice of porous activated carbon powders as the preferred materials of EDLC electrodes [6,7] gives rise to the possibility that the application of a compressing force might change the morphology of the electrode material. This could result in (1) a displacement of the electrolyte away from contact with the surface of the carbon electrodes and (2) a significant decrease in the accessible surface area of the carbon material due to the restriction of the transport channels [8,9]. This would have a significant impact on the performance characteristics of the EDLC [6,10–12].

Our previous work addressed the question as to what is the limit to how much of a compressing force could be applied to an EDLC cell. Those results showed that the application of force on an EDLC cell only provided an average increase of 4.5% in the capacitance of the device as compared to the capacitance prior to the application of force. Any additional force would generally not offer any

* Corresponding author. Tel.: +1 617 287 6036; fax: +1 617 287 6185.
E-mail address: deyang.qu@umb.edu (D. Qu).

0378-7753/$ – see front matter © 2012 Elsevier B.V. All rights reserved.
doi:10.1016/j.jpowsour.2012.04.046

significant improvement and resulted in capacitance values that were, on average, only 1.4% above the initial value prior to the application of force. Furthermore, under certain conditions, the EDLC cell exhibited a substantial loss of performance producing a decrease in the cell's capacitance of between 10 and 84%. It was concluded that the application of force altered the physical structure of the activated carbon electrodes, resulting in a decrease in the accessible surface area and a displacement of the electrolyte, a phenomenon also known as 'electrolyte starvation'. The AC impedance response of an electrode in this state also supported these conclusions, as was seen by the change in the distribution of the total capacitance and the decrease in the values of the individual RC time constants [13].

The goal of this work was to expand upon those previous experiments by evaluating the applied-force response that different carbon material electrodes exhibit. In the manufacturing of a supercapacitor, the assembled device is subjected to a compressing force or to optimize those characteristics as previously noted. Furthermore, during the manufacturing of the electrodes used in the supercapacitor, the final step to form the electrode film is to subject the materials to a high-pressure rolling mill. In both instances, the compressing force could significantly alter the properties of the carbon material, which could have impact on the performance of the supercapacitor. The efforts to understand such impacts are reported in this paper.

In this evaluation, carbon electrodes were prepared from eight different carbons and were tested in triplicate experiments using the same protocols as was previously defined in our prior work [13]. It would be expected that different activated carbons would exhibit different behaviors as a result of variations in their porous structure. Furthermore, it would be expected that those same variations would give rise to differences in the recoverability that the electrode materials would exhibit after the release of that force, where recoverability is defined as to how well the cell returns to its initial level of performance. In addition, the porous structure of the carbon material of the electrode was examined before and after the pressing using porosimetry analysis as a way to understand the changes in its structure that were induced from the application of force. For that latter work, the RP-20 carbon material (Kuraray Chemical) was evaluated because it showed the poorest recovery after the application of force and to provide a comparison, the WPH carbon material (Calgon Carbon) was also evaluated.

2. Experimental details

2.1. Materials

A selection of eight different activated carbons was evaluated and they are listed below in Table 1. For more a detailed description of the experimental procedures, refer to the Experimental section in our prior work [13]. The average electrode mass reported in Table 1 is the mass of the carbon film only; it does not include the mass of the nickel mesh that is the other component of a carbon electrode. It should be noted that the mass of the carbon film includes the mass of the active material (carbon powder) and the mass of the PTFE binder. A porous polymeric membrane (C200, Celgard) was used as the separator and 1 M tetraethylammonium tetrafluoroborate, ($TEABF_4$) in acetonitrile was chosen as the electrolyte for all cells. The $TEABF_4$ salt and acetonitrile (99.9%) were obtained from Novolyte Technologies. The moisture content of acetonitrile was determined to be lower than 5 ppm by Karl-Fisher titration and was used as received.

Table 1
Properties of the activated carbon materials.

Type	Supplier	BET SSA ($m^2\ g^{-1}$)	DFT SSA ($m^2\ g^{-1}$)	Pore size, BET (Å)	Electrode mass (mg)
YP-50F	Kuraray Chemical	1530.0	1283.0	22.1	28.1 ± 1.9
YP-17D	Kuraray Chemical	1643.5	1286.5	22.4	24.5 ± 0.9
M-20	SpectraCorp USA	2130.0	1450.0	22.9	22.1 ± 0.7
A Supra	Norit	1751.4	1326.1	24.6	33.6 ± 0.3
ADP	Calgon Carbon	1232.3	918.0	26.6	21.6 ± 0.6
RP-20	Kuraray Chemical	1568.1	1401.7	21.8	27.9 ± 0.9
SX Ultra	Norit	951.2	861.1	36.8	20.8 ± 0.3
WPH	Calgon Carbon	1153.8	873.4	26.1	27.0 ± 1.1

2.2. Electrodes and test cell

The electrodes were prepared following the same procedure that was described in our previous work. The carbon powders were combined with Teflon, for use as the binder, and prepared into a dough-like material that was hot molded into a flexible film and then subsequently laminated onto a Ni mesh. The cut electrodes were dried under vacuum and then stored in the glove box, with an argon atmosphere, until required. The average final thickness of the electrodes was 0.32 mm and the diameter was 17.6 mm. The cells used in the experiments described in this work used the same configuration that is illustrated in Fig. 2 of our prior work. Although the cells can be tested in either 2- or 3-electrode configuration, the cells in this work were evaluated in a face-to-face, two carbon electrode configuration that is representative of a commercially manufactured capacitor.

For each experiment, the cell was assembled under an argon atmosphere (less than 2 ppm O_2, H_2O). Prior to assembly, the porous separator was immersed in a small amount of electrolyte. A small quantity of the electrolyte was added to each cell half to wet the reference electrode and the supporting nickel base current collectors. The carbon electrodes were placed in position and wetted with electrolyte. The saturated porous separator was placed in position on one of the electrodes and the two cell halves assembled. Additional electrolyte was transferred into the cell cavity through the ventilation hole until the electrolyte expelled any trapped atmosphere out of the cell. The gap between the two cell halves was reduced in a stepwise manner to control the degree of reduction in the gap distance between the two cell halves, with a release of the cell pressure after each reduction. This procedure allowed the electrodes within the cell to experience a slight pressure during assembly, while also preventing that pressure from becoming high enough to damage the electrodes or separator.

The internal configuration of the cell was altered for the force testing experiments by inserting four nickel spacers, each 0.254 mm in thickness, between one of the nickel current collectors and the corresponding Teflon base. This allowed the decrease in the internal gap between the working and counter electrodes to be determined externally while an external compression force was applied to the cell. The external gap between the two cell halves was used to calculate the internal gap between the two electrodes using equation (1). The internal dimensions of the cell were determined prior to these experiments. The EDLC cell was then assembled using the stepwise procedure, while accounting for the increased spacing between the two electrodes introduced by the addition of the spacers. A cell was considered completely closed when the gap between the two cell halves was equal to the combined thickness of the spacers that were added prior to assembly (1.02 mm). This stage marked the starting point for all experiments. The internal gap between the working and counter electrodes was calculated using Eq. (1).

$$\mathrm{Gap_{mm}} = (\mathrm{Gap_{in}} - \mathrm{SP}_h + 0.94\ \mathrm{mm} - h_E \cdot 2) \quad (1)$$

where Gap_{in} is the external gap between the two cell halves, SP_h is the height of the spacers added to interior of the cell, and h_E is the average thickness of one carbon electrode. The value of 0.94 mm represents the unmodified gap between the Ni current collectors.

A compressing force was applied to an assembled cell using a vertical hand wheel Force Testing stand (IMADA model HV-110S) equipped with a digital force gauge (IMADA model DS2). A cell was assembled to its initial starting state and then force was applied to reduce the internal gap between the two cell halves of the cell. This had the effect of decreasing the volumetric capacity of the cell cavity and increasing the pressure on the working and counter electrodes. The decrease in the gap distance between the two cell halves was controlled through the use of stainless steel shims of fixed size. The force applied to the cell and the gap between the two cell halves was also measured and the maximum average force was determined to be approximately 1120 N. Cyclic voltammetry (CV) analyses were periodically performed and when an analysis indicated that one or both of the carbon electrodes had exhibited a substantial morphological change. That state was indicated by a substantial collapse of the CV curve. For a visual example of this compression, please refer to Fig. 4 in the earlier work [13]. If this was indicated, the pressure on the cell was immediately released and the cell returned to its original state. Then, AC impedance and cyclic voltammetry analyses were performed and the results recorded. An example set of typical CV curves is presented in Fig. 1, which shows the CV results at different stages of and YP-17D electrode experiment. Replicate experiments were conducted for each activated carbon to ensure reproducibility.

2.3. Instruments and testing procedures

Linear sweep cyclic voltammetry (CV) analyses were carried out on the cells in the 2-electrode configuration using a Metrohm Autolab potentiostat/galvanostat (PGSTAT30) under a scan rate of 100 mV s^{-1} and through a potential range of −2.0 to +2.0 V. The electrochemical impedance spectroscopy (EIS) analyses were also carried out using the same potentiostat/galvanostat with the frequency analyzer (FRA2) module set to a frequency range of 100 mHz to 10 kHz. The instrument was computer controlled for both tests using the Nova software (version 1.5, Metrohm Autolab B.V.). All equivalent circuit fittings of the EIS data were performed using the ZView software (version 3.3a, Scribner Associates).

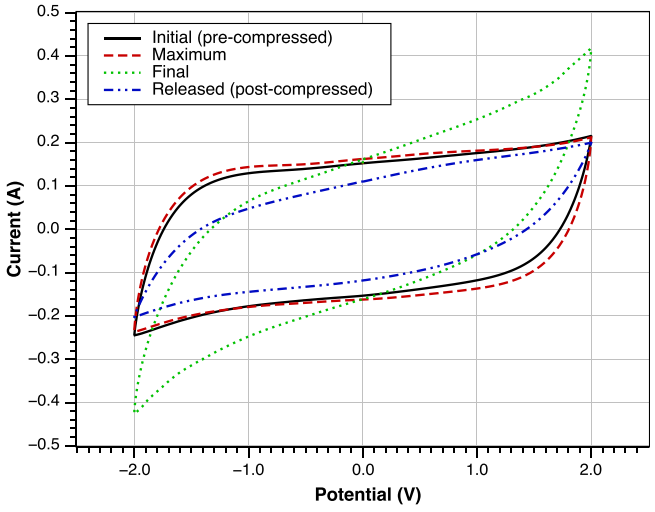

Fig. 1. Typical CV curves. Cyclic voltammetry curves for the cell #1 prepared with the YP-17D electrode material. The data was obtained at the initial (pre-compressed), maximum capacitance (compressed), fully closed (compressed) and fully released (post-compressed) states are represented.

The porosimetry analysis was performed using the Micromeritics ASAP 2020 Surface Area and Porosity Analyzer and nitrogen was used as the absorbent gas. The porosity calculations (surface areas, pore distribution) were determined using density function theory (DFT) with the slit pore geometry. In addition, the Horvath–Kawazoe adsorption model using the slit pore geometry was used to determine the micropore distribution. All calculations were performed by the ASAP 2020 software (version 3.00) supplied by Micromeritics.

For the porosimetry analyses, two pairs cells were assembled using electrodes prepared with either the RP-20 carbon or the WPH carbon, a separator (Celgard C200) and acetonitrile. One cell from each pair was subjected to the same force compression conditions as described previously and kept at that state for 18 h. The other cell of the pair was kept at the initial (pre-compressed) state for the same length of time. Each cell was then disassembled, both electrodes removed, and the electrodes allowed to sit for approximately 10 min to allow the acetonitrile to evaporate. The electrodes were then cut into pieces and placed into a tared sample tube for the porosimetry analysis.

3. Results and discussion

3.1. Cyclic voltammetry (CV) measurements

By comparing the CVs of the same cell under different pressured states, certain observations regarding the total capacitances associated with the cell can be made. The degree of rectangularity in a CV is an indication of how close the performance of a supercapacitor approaches that of an ideal capacitor: the more rectangular the CV, the more the supercapacitor cell approaches capacitor-like behavior. Additionally, it is understood that the average of the absolute values of the charging current and the discharging current is representative of the total capacitance for the cell [4,14]. A capacitance value for the cell can therefore be calculated from the CV data by integrating the current over the entire CV curve and obtaining an average value. Using this value and the scan rate, a capacitance value can be calculated using Eq. (2).

$$\begin{aligned} q &= C\cdot V \Rightarrow \frac{\delta}{\delta t}q = \frac{\delta}{\delta t}(C\cdot V) \\ \frac{\delta q}{\delta t} &= I = C\frac{\delta}{\delta t}V \\ I &= C\cdot s \end{aligned} \tag{2}$$

where I is the current in amperes, C the total capacitance in Farads, and s the potential sweep rate (V s^{-1}).

The same behaviors that were observed in the CV measurements in the previous work [13] were also seen in the measurements of the cells used in these experiments. Specifically, as more force was applied to an EDLC cell, the capacitance increased until a maximum value was reached. After which the calculated value for the capacitance, either stopped increasing and maintained a relatively constant value, or decreased as additional force was applied to the cell. This is illustrated in Fig. 1, which shows four CV curves from different stages of the experiments conducted using the YP-17D carbon material. Fig. 1 clearly shows that the cell capacitance reaches a maximum with the application of some compressing force ('Maximum'), but with increasing force there is a decrease in the cell capacitance ('Final'). After the compression force is released, the appearance of the CV curve indicates a decrease in performance ('Released').

The summarized results for the different electrode materials are shown in Fig. 2. The bars in the figure represent the percent change in the cell capacitance with the application of a compressing force with respect to the capacitance value calculated when the cell was in its 'Initial' state. The bars labeled 'Maximum Increase' indicate the maximum increase in the cell capacitance whereas the bars labeled 'Maximum Decline' indicate the maximum decrease in the cell capacitance, after the maximum value, with the continued application of force. Both the 'A Supra' and 'SX Ultra' cells show large declines with wide standard deviations in the average values. This is not unexpected since either small or large decreases in the cell's capacitance can occur with the application of the compressing force. Therefore the average value for the decrease in the capacitance can show significant variability.

As stated in the Introduction, electrode films prepared from carbon powder material would be expected to possess a sponge-like quality due to the porous nature of activated carbons. Therefore, it would be expected that the material would return to a structural state very similar to the initial state it possessed prior to being subjected to a compressing force. However, the results of this work show that this is not always the case. When the compressing force was removed from the cell and the internal cell gap returned to its initial value, the cells were again analyzed using cyclic voltammetry and electrochemical impedance spectroscopy and capacitance values calculated from the CV curves. Those results showed that, after the release of the compressing force, the electrodes prepared from some of the activated carbons exhibited capacitance values that were significantly less than the capacitance value calculated when the cell was in its initial state. An average percent recovery, as compared to the initial capacitance value, was calculated for each carbon electrode and is plotted in Fig. 3.

Fig. 3 shows that only the electrodes prepared from four of the carbons demonstrated recoveries close to 100%: A Supra, ADP, WPH and SX Ultra. However, the electrodes made from the other carbons, M-20, RP-20, YP-17D and YP-50F, produced recoveries significantly less than 100%, with some as low as 50% recovery. Since all of the electrodes were prepared using the same procedure, it can only be concluded that these differences must arise from the nature of the carbon materials themselves. To gain further insight into this behavior, it was decided to perform porosimetry analyses of an electrode before and after being subjected to thee compressing force.

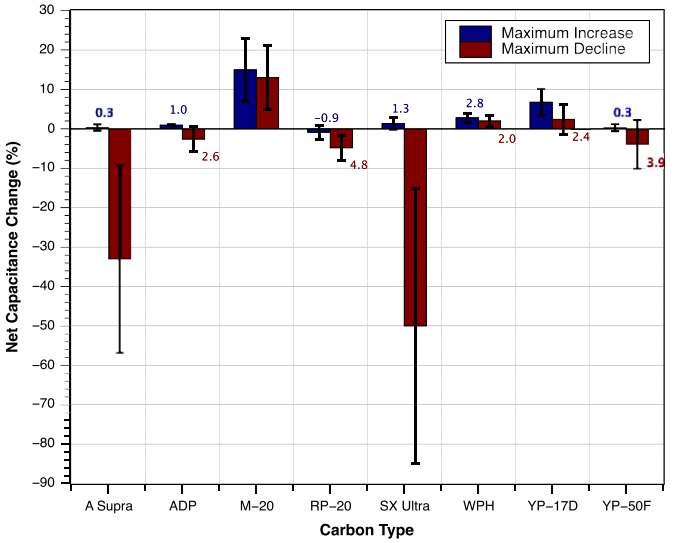

Fig. 2. Change in capacitance with internal gap. The change in the specific capacitance from the initial value as determined at the reference state. The 'Maximum Increase' refers to the maximum increase in the cell's capacitance value after the application of the compression force. The 'Maximum Decline' refers to the maximum decrease in the cell's capacitance value after reaching the 'Maximum Increase' stage.

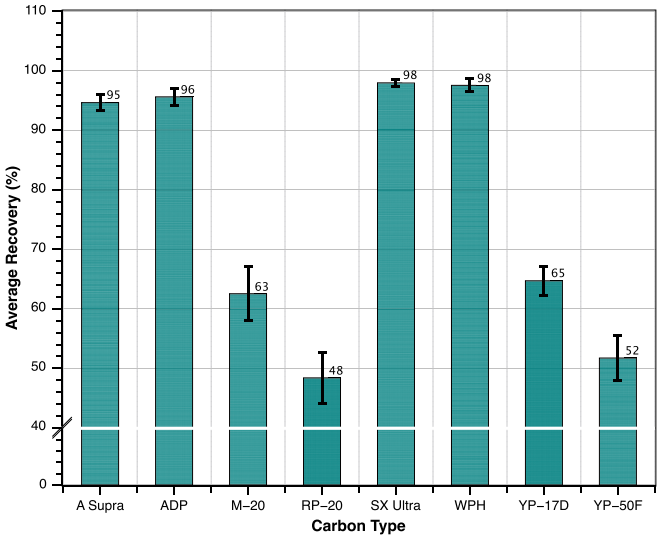

Fig. 3. Percent recovery of initial capacitances. The post-compression response of the cell as determined by comparing the post-compression CV capacitance values as percentages of the capacitance value calculated when the cell was in its initial state.

3.2. Porosimetry analyses

The RP-20 (Kuraray Chemical) activated carbon was chosen for the porosimetry analyses because it demonstrated the most significant loss in capacitance, as compared to the initial state, after being subjected to a compressing force. To provide a comparison, a porosimetry analysis was also performed on the WPH (Calgon) activated carbon. Electrodes prepared with that particular carbon demonstrated a minimal loss in its capacitance after the release of the compressing force. Rather than exposing the electrodes to electrolyte, as would be the case in a normal cell, only acetonitrile was used. This eliminated any possible concerns about residual salts that may have been left on the electrodes if actual electrolyte was used. The carbon electrodes were tested at two different stages in the pressure experiment process: before and after the application of pressure. The cumulative surface area as a function of the pore diameter for the WPH and RP-20 sets of electrodes are presented in Fig. 4a and b, respectively.

The porosimetry results for the WPH carbon electrodes only show some slight changes in the contribution to the total surface area by pores in the 6–7 Å range, but those differences are not significant. However, a comparison of the results for the 'Pre-compressed' and 'Post-compressed' states for the RP-20 carbon shows more significant changes and yields two observations. The post-compression electrode now shows a significant contribution to the surface area from pores with widths of approximately 5.0 Å. This results in a decrease in the contribution to the total surface area by pores with widths greater than 5.5 Å. When the cumulative surface area of both electrodes is plotted as a function of pore width, the results from the post-compression electrodes shows a downward shift toward smaller pore widths in the pore distribution as compared to the results from the pre-compression electrode, as shown in Fig. 4a. This indicates that more of the total surface area is associated with the smaller pores than was the case in the electrode prior to being subjected to compression. With the application of force to the porous structure of the carbon material,

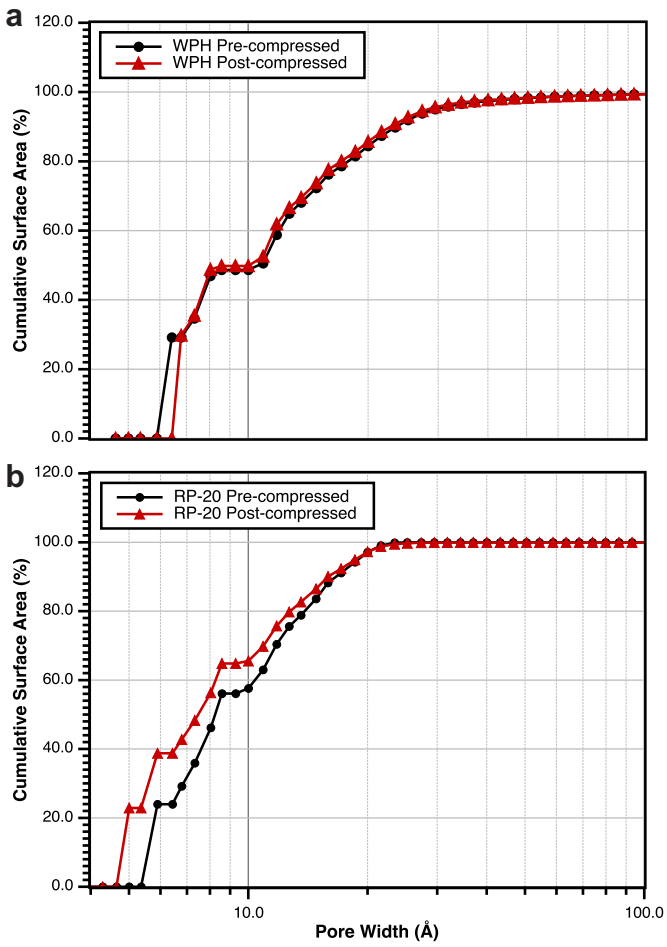

Fig. 4. Cumulative surface area. Cumulative surface area, as calculated by DFT, of the RP-20 (a) and WPH (b) electrode materials before and after the application of force. Pores with widths greater than 40 Å did not significantly contribute to the total surface area and, as such, did not demonstrate any substantial changes after the application of the compression force.

that structure is compressed and the geometries of the pores are changed. Using the pore distribution results from the DFT analysis, a mean pore width can be determined through a summation of the pore widths weighted by their contribution to the total surface area, as shown in Eq. (4), where r_n, A_n, and A_s are the pore width, incremental surface area, and total surface area, respectively, of the pores as determined by the DFT analysis.

$$W_p = \sum_{n=1}^{N} r_n \left(\frac{A_n}{A_s}\right) \quad (3)$$

Average pore width values were calculated for the pressed and un-pressed electrodes using Eq. (3) and are reported in Table 2. A comparison of those values confirms that the average pore width for the RP-20 had decreased in the post-compressed electrode from the value in the pre-compressed electrode by approximately 10%, whereas the average pore width value for the WPH electrodes has only decreased in the post-compressed electrode by approximately 1%.

It has to be noted that the values for the total specific volume and specific surface area reported in Table 2 cannot be considered to represent the actual specific volume or specific surface area of the carbon material, since the electrodes that were analyzed by porosimetry include the nickel mesh current collector to which the carbon film was laminated. The mass of that component contributes significantly to the total mass of the electrode but not to the overall volume or surface area as determined by the analysis, which would result in artificially low values. However, since the size and the weight of the current collectors were the same, the differences in the total pore volume and the total surface area indicate that there were changes in the pore dimensions.

Table 2
Average pore widths for the pressed and un-pressed electrodes as calculated from the total pore volume and total surface area using Eq. (5).

DFT analysis	Total pore volume ($cm^3 \cdot g^{-1}$)	Total surface area ($m^2 \cdot g^{-1}$)	Avg. pore width (nm)
RP-20 Electrode			
Un-pressed	0.1771	332.7	1.065
Pressed	0.2065	429.9	0.961
		% Change	−9.8
WPH Electrode			
Un-pressed	0.1444	200.5	1.440
Pressed	0.1519	213.2	1.425
		% Change	−1.0

While a definitive lower size limit of pores that can be accessed by organic electrolytes has yet to be determined, it can be expected that a portion of a carbon material's micropores (i.e., pores <20 Å) must be accessible to organic electrolytes, when considering the high capacitance values regularly reported for highly microporous carbons. On the other hand, the electrode material capacitance observed with aqueous electrolytes is typically greater than the value in an organic electrolyte. This difference is generally attributed to the smaller overall diameter of the solvated aqueous electrolyte ions, which would allow greater access to the smaller pores. However, studies on micropore accessibility in aqueous solvents have concluded that, generally, pores 5 Å or smaller are not available for the adsorption of hydrated ions [15–17]. Therefore, it is safe to conclude that the surface area associated with the 5.0 Å pores cannot be considered as being electrochemically accessible.

Additional information can be obtained by examining the distribution of micropores obtained by using Horvath–Kawazoe model [18,19]. The analysis produced a listing of the cumulative pore volume with increasing pore width. An incremental pore volume distribution was calculated from that data and the results are shown in Fig. 5a and b for the WPH and RP-20 electrodes, respectively.

Overall, the pore volume values for the WPH electrodes are somewhat less than the ones for the RP-20 electrodes. This is not unexpected since its smaller total surface area and generally larger average pore diameter are an indication that the WPH carbon possesses less microporosity than the RP-20 carbon (see Table 2 and Fig. 4). Overall, the plots in both figures show a decrease in the pore volume contribution with increasing pore width, but also a region of increased pore volume in the 8–12 Å range. In comparing the results for the WPH electrodes before and after compression of the cell, there is an increase in the total pore volume contribution by pores with pore widths of approximately 9.5 Å and a slight redistribution of the pore volume contributions associated with the pores in the 8–12 Å pore width range. Similar, but more significant changes are evident in the results for the RP-20 electrodes. In that case, the electrode that was subjected to the compressing force shows a decrease in the total pore volume contribution by pores of approximately 9.5 Å pore widths. Again, there is a redistribution of the pore volume contribution in that same 8–12 Å pore width range, but in general, there is a decrease in their contributions to the total pore volume. The differences in the plots of the micropore distribution indicate that the application of

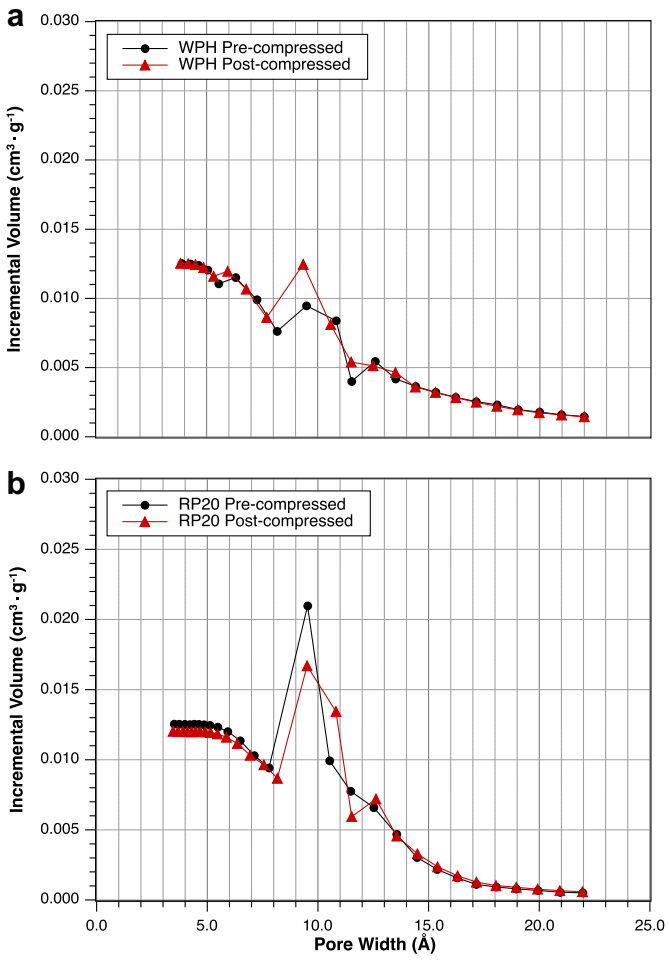

Fig. 5. Micropore distribution. Micropore distribution, as calculated using the Horvath–Kawazoe model, of the WPH (a) and RP-20 (b) electrode materials before and after the application of the compression force.

the compressing force induced changes in the distribution of the pore volumes of the carbon electrodes. The decrease in the pore width and the changes in total surface area for the RP-20 electrode coupled with the changes seen in the micropore distribution seem to indicate that the compressing force resulted in a more significant alteration of the internal pore structure than what was evident for the WPH electrode.

In a porous carbon electrode, the majority of the pores available for the electrolyte are the inter-particle spaces formed by the aggregation of carbon micro-domains. It has previously been reported that at elevated pressures, the fluid in the smallest pores of a porous material can induce volumetric deformations of the material's porous structure [20,21]. Therefore, it is not unreasonable to expect that the application of an external compressing force on the electrolyte-filled pores of an electrode will exhibit a similar effect, compressing the aggregated micro-domains. It is expected that the compressed aggregated micro-domains would eventually 'spring-back' after the compression is released restoring the pore structure back to a state that is similar to its initial state. It has been reported by Hahn [22] that, for activated carbon materials with sufficient graphitic character, there is a significant potential for the insertion/de-insertion of electrolyte ions into the carbon matrix during the cycling of a supercapacitor cell. This process results in volumetric changes of the electrode, not unlike what is seen during the intercalation/de-intercalation process of graphite materials [23]. This would introduce additional stress on the carbon matrix, which would be intensified if that matrix was under pressure. While in the compressed state, the carbon aggregates could exhibit one or more different behaviors, of which we will only discuss a few here. In one possible scenario, during the process of compressing the electrode, hetero materials that are adsorbed on the surfaces could shift or be displaced allowing access to those microporous surfaces that had previously been 'covered'. This would be evidenced by an increase in the micropores. In another scenario, the compressing force could result in a reorientation of the primary collection of micro-domains forming new aggregate collections. The pores formed by the new arrangement of the aggregated micro-domains might have a smaller average pore width and, due to the increase in the microporosity, result in an increase in the total surface area. This latter modification would result in a new permanent state. Since a long-term study to determine the permanency of these changes has not been completed, it would not be prudent at this time to definitively attribute their ultimate cause. However, it can be stated that a smaller average pore width would result in a general decrease in the accessibility of a significant portion of the total surface area. However, it would be very difficult to assess what effect the changes in the porosity of the carbon electrodes will have on the performance of the supercapacitor based on the results of the porosimetry analyses alone, since that analysis uses an adsorbate gas as a means to determine accessibility. It is well known that a certain portion of the surface area of a porous material, as determined by porosimetry, will be less accessible in an electrochemical environment since electrolyte ions, and their associated solvation spheres, cannot be expected to access all of the same surfaces that an adsorbate gas can [9,17,24]. A more in depth understanding of the electrochemical accessibility of these altered materials can be achieved by evaluating the results of the EIS analyses.

3.3. Electrochemical impedance spectroscopy analyses

Electrochemical impedance measurements were conducted to aid in determining the electrochemical accessibility of the carbon electrodes after being subjected to the compressing force. The impedance analysis was conducted at the open cell potential with an AC amplitude of 5 mV. The spectra were measured over a frequency range of 10 mHz–100 kHz before, during, and after the cells were subjected to the compressing force. Typical Nyquist plots for the RP-20 electrode at these different states are presented in Fig. 6.

As would be expected when comparing the impedance spectra of the pre-compression and compressed cell, there is a noticeable leftward shift in the data that represents a decrease in the impedance. This can be attributed to a decrease in the equivalent series resistance (ESR) of the cell. The ESR arises out of the contact resistance between the electrode and separator and inter-particle resistance of electrode material and it is expected to decrease with the application of the compressing force. In general, the impedance spectra obtained at those two states show the data as a combination of a very small, depressed semicircle at high frequencies and a steep sloping line that approaches verticality in the medium to low frequency range. This is typical for a supercapacitor [1]. After the compressing force was released and the cell returned to the initial state, the impedance analysis produced a spectrum that shows a dramatic change from the one obtained from the initial state cell. There is now a large, depressed semicircle covering the high and medium frequency range with a shorter, steeply sloping line in the low frequency range. The changes exhibited in the spectrum will arise out of a combination of two

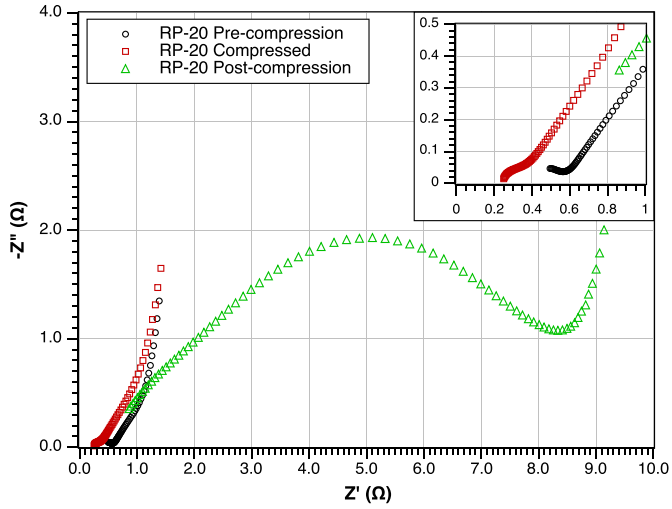

Fig. 6. Nyquist plots. The impedance data obtained at the open cell potential from one cell assembled using the RP-20 electrode using an AC amplitude of 5 mV. The data was obtained at the pre-compressed (○), compressed (□), and post-compressed (△) state.

factors: (1) a decrease in the apparent capacitance and (2) an increase in the resistance of the cell.

The impedance response of a supercapacitor cell constructed with porous electrodes can be modeled using the transmission line equivalent circuit [1,25], as represented in Fig. 7.

The infinite transmission line model used to fit the data generated from the experiments in this work was truncated to an 8-loop model to simplify the fitting. The results from the EIS analysis can be used to show the changes in ESR value for the cell with the application of the compressing force. A summary of the results obtained from all carbon electrode types shows that there was an average decrease of between 35 and 60% in the calculated ESR value with the increase in force on the cells. For the analysis of the RP-20 electrodes cell specifically, the ESR decreased from 0.42 to 0.27 Ω. A similar trend was observed for the WPH electrodes: from 0.43 to 0.16 Ω. As expected, the calculated ESR values for the post-compressed state show an increase from both the compressed state and the pre-compression state values. However, for the RP-20 and WPH electrodes the post-compression values were determined to be only 0.66 and 0.61 Ω, respectively. This corresponds to increases of 57% and 42% as compared to the pre-compression values. It is clear then that the increased resistance of the cell cannot be attributed to changes in the ESR alone.

The modeled response of an RC transmission line network is analogous to the depth that an AC signal may penetrate with respect to the depth of the pores. Therefore, different sized pores in a porous electrode will have different time constants, which can be correlated to electrolyte ion access times, as elaborated by Lozano-Castello [17] and others [7,14,24]. The implication is that not all of the accessible surface area of a porous electrode can be accessed within the same time frame and the maximum capacitance will depend upon the density of the charging current or modulating frequency [4,9,12]. The diffusion rates of ions into and within the different sized pores will vary with the frequency, which directly

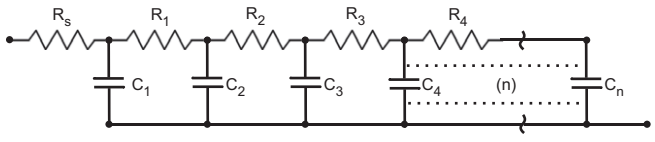

Fig. 7. Generalized transmission line network. The equivalent circuit used in this work is a truncated version that consists of eight RC loops.

impacts the response times of the double-layers established on the surfaces of those accessed pores. Higher frequencies only allow the electrolyte ions to access the more easily accessible surface area, which will correspond to the pores with the widest dimensions and the external surfaces [26]. Conversely, lower frequencies of the modulating signals, with longer time scales, will project both the accessibility and the surface area of the smaller pores due to the increased access time [27–29].

In the transmission line model, the indices of the different RC loops correlate to the accessibility and the changes of the accessible surface area associated with different sized pores under different conditions. Changes in the resistance of the resistor of each individual RC loop (a sub-resistor, R_n) are associated with a change in the ability to access the specific surface area. Such resistivity could come as a result of the ohmic and diffusion resistances of ions in pores of different sizes, whereas changes in the capacitance of the capacitor in the different RC loops (a sub-capacitor, C_n) will inversely correlate to changes in the projected surface area of the different sized pores, from largest to smallest.

Our previous work established that subjecting a supercapacitor cell to a compressing force induced a change in the distribution of the capacitance among the different sub-capacitors. The contribution to the total capacitance from the sub-capacitors that can be considered to represent the mesopores and the larger-sized micropores decreased and the share associated with the smaller-sized micropores increased. That share represents the 1/8 fraction of the total accessible surface area contributed by the smallest pores. That change in the distributed capacitance distribution was caused by an alteration in the accessible surface area of the various sized pores. The electrochemical accessibility to those pores decreased, which came as a result of the loss of electrolyte from within those pores, or 'electrolyte starvation', where there is an insufficient density of electrolyte ions to firmly establish a double layer [14,30].

The data from the electrochemical impedance spectroscopy analysis of the cells prepared with the RP-20 carbon electrodes was fitted to an 8-loop equivalent circuit and values for the individual sub-resistors and sub-capacitors were calculated. Since the sub-capacitors in the transmission line model are in parallel, the total capacitance can be calculated through a simple summation of the individual sub-capacitors (see Eq. (4)), which was used to calculate an individual sub-capacitor's contribution to the total capacitance.

$$\frac{1}{Z_{\text{img}}} = \sum_{1}^{8} \frac{1}{Z_{\text{cap}_n}} \Rightarrow \frac{1}{1/j\omega C_{\text{tot}}} = \sum_{1}^{8} \frac{1}{1/j\omega C_n}$$
$$j\omega C_{\text{tot}} = j\omega \sum_{1}^{8} C_n \Rightarrow C_{\text{tot}} = \sum_{1}^{8} C_n \quad (4)$$

Fig. 8 was generated from those results. Fig. 8a shows a plot of the resistance values for each individual sub-resistor (R_1 to R_8) and Fig. 8b shows a plot of the capacitance values of each individual sub-capacitor (C_1 to C_8) as a percentage of the total capacitance for both the RP-20 and WPH electrodes.

As was seen in previous figures (see Figs. 4 and 5), the results for the WPH electrode show only slight differences between the pre-compression and post-compression states. This would seem to indicate that the compression force did not significantly affect the distribution of the total resistance and total capacitance. However, the same cannot be observed for the RP-20 electrode. Overall, there was an increase in the resistance values for the individual sub-resistors and a shift in the distribution of the capacitance contributions to the less accessible pores.

The porosimetry data showed that the application of force to the electrode by a compression of the supercapacitor cell resulted in a change in the electrode material's morphology. This produced an

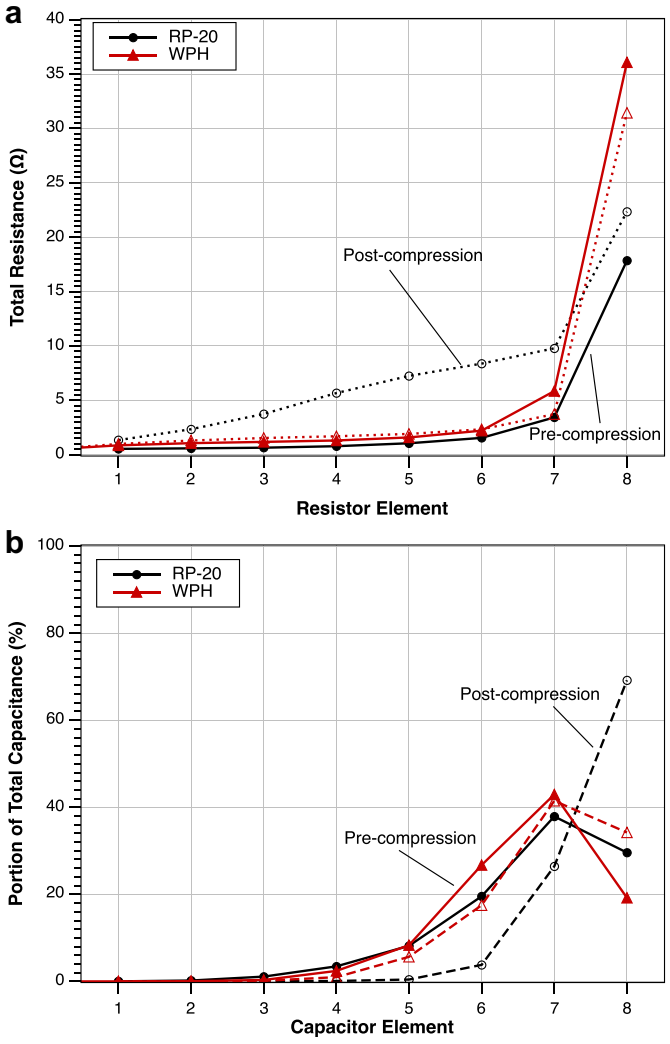

Fig. 8. Distribution of resistance and total capacitance for RP-20 electrode. Distribution of the numerical resistance associated with each sub-resistor (a) and distribution of the total capacitance associated with each sub-capacitor (b) as calculated from a fitting using the equivalent circuit shown in Fig. 7.

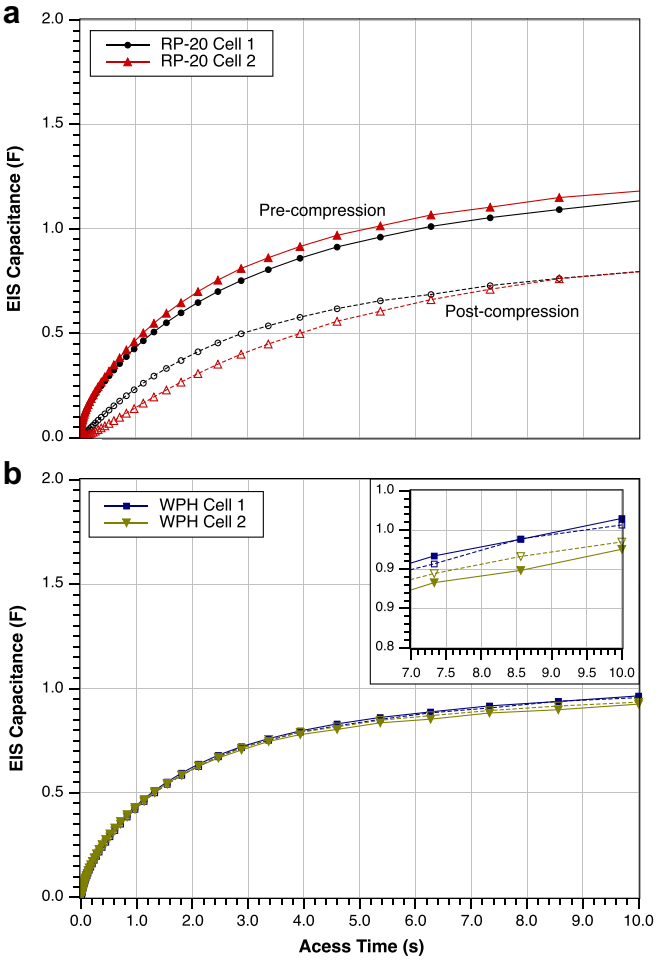

Fig. 9. Cumulative EIS capacitance of RP-20 and WPH electrodes. Cumulative EIS capacitance values calculated from the imaginary component of the impedance for the pre-compressed and post-compressed electrodes prepared from the RP-20 carbon (a) and the WPC carbon (b). Solid lines: pre-compression, dashed lines: post-compression.

alteration in the distribution of the pore volumes for pores in the micropore range (<20 Å). The net effect was a decrease in the electrochemical accessibility, which can be correlated with an increase in the total resistance. This is illustrated as an increase in the resistance values associated with each individual sub-resistor, as is shown in the EIS results presented in Fig. 8a. Within certain time scales, this increased resistivity would result in a decrease in the apparent capacitance due to a drop in the contribution by the individual sub-capacitors toward the total capacitance. This results in a shift in the distribution of the capacitance values toward the smaller-sized pores that are only accessible within longer time scales (or lower frequencies) [9]. Therefore, lower frequencies are required to allow sufficient time to establish the double layer on the less accessible surface area of those pores. This is apparent by the calculated results shown in Fig. 8b: more of the total capacitance is attributable to the smaller-diameter pores in the post-compressed electrode than in the pre-compressed electrode.

In addition, an examination of the raw impedance data presents an opportunity to corroborate the results and conclusions drawn from the porosimetry data. With the assumption that there is no contribution to the impedance from Faradaic processes, the total impedance of the system can be separated into a real part and an imaginary part [31–33]. The real part can be correlated with the resistances of the system and the imaginary part to the capacitances of the system, respectively (see Eq. (5))

$$Z_{\text{tot}} = Z_{\text{real}} + Z_{\text{imag}}$$
$$Z_{\text{real}} = R \text{ and } Z_{\text{imag}} = \frac{1}{j\omega C} = -\frac{j}{2\pi f C} \quad (5)$$

In a typical EIS analysis, the impedance of the system is determined over a range of frequencies, out of which the two component parts are typically generated. In this system, capacitance values as calculated from Eq. (5) can be interpreted as a reflection of the potential double layer than can form on those surface areas that are accessible at that analysis frequency. Therefore, the reciprocal of the frequency corresponds to the time allowed for the electrolyte ions to access any particular surface, and so with an increase in the access time (or decrease in frequency), ions can reach those surfaces that are less accessible to form a double layer [24,26]. So as access time increases, more of the surface area of the electrode is being accessed, and the most difficult surface areas to access correspond to the smallest pores in a porous material. By examining how these calculated EIS capacitance values change with increasing access time, the contribution that those surface areas make toward to the cumulative capacitance can be measured on an

individual basis. From the EIS analysis, the capacitance values obtained from the imaginary portions of the impedance data for each individual frequency were calculated using Eq. (5). The results from the RP-20 and WPH experiments were plotted as a function of the access time, or reciprocal frequency, and are shown in Fig. 9a and b, respectively.

The *x*-axis can be interpreted by understanding that an increase in time corresponds to a decrease in the accessibility of the surface and the capacitance plotted along the *y*-axis can be seen as a reflection of the surface area that can be accessed within that particular time-scale. It is clearly demonstrated by the electrode prepared with the RP-20 carbon (Fig. 9a), that a longer time is required to access the same surface area or to achieve the same capacitance for the post-compression electrode than for the pre-compression electrode. This change in behavior can be attributed to the morphological changes that arose out of the compression of the porous electrode material, as discussed above. This observation matches well with the changes in the pore distribution as indicated by the porosimetry analyses (refer to Figs. 4 and 5). Such modifications of the carbon material resulted in a decreased capacitance value for the post-compression RP-20 electrode as shown in Fig. 3. Conversely, the data presented in Fig. 9b indicates that, although the WPH electrodes experienced similar physical stresses during the experiment as the RP-20 electrodes, the WPH carbon material did not exhibit the same behavior. Furthermore, this observation can be extended to those carbons that did not show a significant decrease in their post-compression capacitance values (see Fig. 3).

Overall, the decrease in the capacitance calculated from the EIS results can be attributed to an increase in the time required to access the more restricted surfaces areas that arose out of modifications to the porous structure due to the compression of the electrode. This correspondence between changes in the access time impacting the ability to establish a double layer can be extended to the results from the cyclic voltammetry (CV) analyses. Different frequencies used in an EIS analysis can be correlated to the scan rates used to conduct a CV analysis. Just as with lower frequencies, slower scan rates would allow more time for the electrolyte ions to access the less accessible surface areas of the restricted pores [2,16,34].

Based on the preceding discussion, a few observations can be made. It can be surmised that the scan rate used for the CV analyses conducted in this work changes the potential too quickly to sufficiently access all of the electrochemically accessible surface areas to establish a significant double layer in the provided time-frames [3,10]. Furthermore, it is reasonable to conclude that, for those electrodes that demonstrated a reduction in their post-compression capacitance, a portion of the porous material's surface area that was previously accessible, was no longer electrochemically accessible in the post-compression state. This would result in a negative impact on the capacitance of the cell. Finally, for those electrodes that did not show a significant reduction in their post-compression capacitance, any alteration of their porous structure was not significant enough to result in a decrease in their electrochemically accessible surface areas. These observations are in a good agreement with what we had reported previously [13].

4. Conclusion

The responses that different carbon material electrodes exhibited to a compressing force were evaluated. The results further substantiated the conclusions that were drawn in our previous work: the application of a compressing force on an EDLC cell only provides a limited increase in the capacitance of the device. Any additional increase in the compressing force does not provide any significant improvement and will, at times, result in a decrease in the cell's capacitance. However, it was also shown that different activated carbons exhibited different behaviors after the compressing force was applied to the electrodes. Those exhibited differences come as a result of variations in their porous structure and it is those same variations that gave rise to differences in the degree to which the cell was able to recover to its initial level of performance after the release of the compression force.

The proximate cause was determined to be that the compression force altered the morphology of the porous electrode in such a way that it induced a modification of material's pore distribution, with the greatest affect in the micropore range. The alteration of the porous structure resulted in a displacement of the electrolyte out of the now more restricted pores. For those electrodes that exhibited the substantial decrease in their post-compression capacitance, these physical changes resulted in a decrease in the electrochemically accessible surface area. This was evident macroscopically as a decrease in the capacitance of the post-compression cell. What remains to be addressed is how the properties of the different activated carbons give rise to the difference seen in their performance recoverability after the application of force.

Acknowledgments

The authors gratefully acknowledge the support from the Office of Naval Research.

References

[1] B. Conway, Electrochemical Supercapacitors: Scientific Fundamentals and Technological Applications (1999).
[2] J. Zheng, J. Huang, T.R. Jow, J. Electrochem. Soc. 144 (1997) 2026–2031.
[3] A. Burke, J. Power Sources 91 (2000) 37–50.
[4] P. Taberna, C. Portet, P. Simon, Appl. Phys. A: Mater. Sci. Process. 82 (2006) 639–646.
[5] R. Kötz, M. Carlen, Electrochim. Acta 45 (2000) 2483–2498.
[6] J. Gamby, P.-L. Taberna, P. Simon, J.-F. Fauvarque, J. Power Sources 101 (2001) 109–116.
[7] D. Qu, H. Shi, J. Power Sources 74 (1998) 99–107.
[8] H. Yamada, I. Moriguchi, T. Kudo, J. Power Sources 175 (2008) 651–656.
[9] A.G. Pandolfo, A.F. Hollenkamp, J. Power Sources 157 (2006) 11–27.
[10] T.-C. Weng, H. Teng, J. Electrochem. Soc. 148 (2001) A368–A373.
[11] Y. Maletin, P. Novák, E. Shembel, V. Izotov, N. Strizhakova, A. Mironova, V. Danilin, S. Podmogilny, Appl. Phys. A: Mater. Sci. Process. 82 (2006) 653–657.
[12] S. Alvarez, M. Blancolopez, A. Mirandaordieres, A. Fuertes, T. Centeno, Carbon 43 (2005) 866–870.
[13] G. Gourdin, A. Meehan, T. Jiang, P. Smith, D. Qu, J. Power Sources 196 (2011) 523–529.
[14] M. Arulepp, L. Permann, J. Leis, A. Perkson, J. Power Sources 133 (2004) 320–328.
[15] G. Salitra, A. Soffer, L. Eliad, Y. Cohen, D. Aurbach, J. Electrochem. Soc. 147 (2000) 2486.
[16] H. Shi, Electrochim. Acta 41 (1996) 1633–1639.
[17] D. Lozano-Castelló, D. Cazorla-Amorós, A. Linares-Solano, S. Shiraishi, H. Kurihara, A. Oya, Carbon 41 (2003) 1765–1775.
[18] G. Horváth, K. Kawazoe, J. Chem. Eng. Jpn 16 (1983) 470–475.
[19] A.P. Terzyk, P.A. Gauden, G. Rychlicki, R. Wojsz, Carbon 36 (1998) 1703–1706.
[20] G. Pijaudier-Cabot, R. Vermorel, C. Miqueu, B. Mendiboure, C. R. Mec. 339 (2011) 770–778.
[21] P. Kowalczyk, A. Ciach, A.V. Neimark, Langmuir 24 (2008) 6603–6608.
[22] M. Hahn, O. Barbieri, F.P. Campana, R. Kötz, R. Gallay, Appl. Phys. A: Mater. Sci. Process. 82 (2005) 633–638.
[23] R. Santhanam, M. Noël, J. Power Sources 66 (1997) 47–54.
[24] L. Permann, M. Lätt, J. Leis, M. Arulepp, Electrochim. Acta 51 (2006) 1274–1281.
[25] J. Bisquert, Phys. Chem. Chem. Phys. 2 (2000) 4185–4192.
[26] H.-K. Song, Y.-H. Jung, K.-H. Lee, Le.H. Dao, Electrochim. Acta 44 (1999) 3513–3519.
[27] L. Wang, M. Fujita, M. Inagaki, Electrochim. Acta 51 (2006) 4096–4102.
[28] L. Wang, M. Toyoda, M. Inagaki, New Carbon Mater. 23 (2008) 111–115.
[29] A. Jänes, L. Permann, P. Nigu, E. Lust, Surf. Sci. 560 (2004) 145–157.
[30] W.G. Pell, B.E. Conway, J. Electroanal. Chem. 500 (2001) 121–133.
[31] M.E. Orazem, B. Tribollet, Electrochemical Impedance Spectroscopy, first ed. Wiley-Interscience, Pennington, 2008.
[32] R. Antaño-Lopez, M. Keddam, H. Takenouti, Electrochim. Acta 46 (2001) 3611–3617.
[33] M.L. Tremblay, M.H. Martin, C. Lebouin, A. Lasia, D. Guay, Electrochim. Acta 55 (2010) 6283–6291.
[34] B. Conway, J. Electrochem. Soc. 138 (1991) 1539–1548.